# Two dominant timescales of cytoskeletal crosslinking in the viscoelastic response of the cytoplasm

Ora T. Cohen and Adam G. Hendricks
*Department of Bioengineering, McGill University, Montréal H3A 0E9, Canada*

(Received 30 July 2022; accepted 13 November 2022; published 6 December 2022)

Cells precisely regulate their frequency-dependent viscoelastic properties in response to chemical and mechanical cues. We use optical trap-based active microrheology using intracellular probes to measure the cytoplasmic mechanical response of fibroblast and macrophage cells over a broad frequency range (∼0.02–350 Hz). Both cell types show similar frequency-dependent behavior, suggesting that the mechanisms that control the cell's mechanical response are general to many cell types. At frequencies above 1 Hz, the cytoplasmic mechanical behavior shows a broad distribution of relaxation timescales consistent with power-law mechanics. At low frequencies (<1 Hz), cells exhibit fluidlike behavior with distinct relaxation timescales, similar to that observed in reconstituted networks of transiently crosslinked actin filaments. The response across all frequencies can be captured by a mathematical model combining a power-law term with two crosslinker-unbinding terms. The two unbinding rates required to describe the low-frequency response suggest that the viscoelastic relaxation of the cytoplasm is governed either by multiple dominant crosslinkers or by a single crosslinker with multiple states.

DOI: 10.1103/PhysRevResearch.4.043167

## I. INTRODUCTION

Cells tightly regulate their mechanics as abnormal cellular mechanics are implicated in cancer, scleroses, and fibroses [1–6]. Cells adapt their mechanics to their environment, behavior, and function [7–10]. Further, cells tune their mechanical response over different timescales [11,12]. Over short timescales, elastic properties dominate the cell's viscoelastic response, while viscous properties become increasingly dominant at longer timescales [11,12]. This frequency-dependent behavior has given rise to various theories attempting to mathematically describe the cell's viscoelastic response, such as poroelasticity, tensegrity, Kelvin-Voigt, and Maxwell models, each posing different explanations for the governing mechanism behind the cell's mechanical behavior [13–16]. Each of these models describe cellular mechanics in specific systems well, yet it has been challenging for any one model to capture the diverse behavior observed across cellular and reconstituted systems.

Power-law mechanics have often been used to describe the viscoelastic response of living cells, indicating a broad range of relaxation timescales [17–22]. Multiple relaxation timescales may be due to the presence of cytoskeletal crosslinkers with varying kinetics, entropic cytoskeletal filament fluctuations, and large-scale network rearrangements [21,23–25]. In contrast, reconstituted systems consisting of actin filaments and a single transiently binding crosslinker exhibit fluidlike behavior at distinct timescales corresponding to the crosslinker unbinding rate [26–30], hereafter referred to as relaxation rate or relaxation timescale. At frequencies faster than the crosslinker unbinding rate, the network exhibits the stiff, solidlike behavior of a statically crosslinked polymer network, while at frequencies near the crosslinker unbinding rate, the network exhibits more fluidlike and viscous behavior as dynamic crosslinker detachments allow the network to rearrange [31]. Only at timescales fast enough to render crosslinker unbinding irrelevant do these networks exhibit the power-law behavior expected of entangled, noncrosslinked networks [31–36]. To describe the low-frequency relaxation and high-frequency elastic behavior observed in dynamically crosslinked polymer networks, the dynamic crosslinking model (DCM) was proposed which combines a dynamic crosslinking term and a power-law term [31].

Although dynamic crosslinking describes the mechanics of reconstituted systems consisting of filaments and crosslinkers well, it has been difficult to perform measurements at the slow timescales corresponding to crosslinker unbinding dynamics in living cells. Using an optical stretcher to measure the mechanics of suspended fibroblasts, Wottawah *et al.* found that their mechanical response exhibited relaxation at a distinct timescale and could not be fit to a power law [37]. Similarly, distinct relaxation timescales were observed in our previous mechanical measurements taken over a broader frequency range in adherent fibroblasts via optical-trapping microrheology [38]. Unlike the power-law behavior of the high-frequency mechanics, we observed a distinct relaxation at low frequencies that was better described by a dynamic crosslinking term, where the timescale of relaxation corresponded to the unbinding rate of the actin crosslinking protein alpha-actinin-4 [38]. While the dynamic crosslinking model captured the fast and slow dynamics well, it was not able to fully describe the experimental data at intermediate frequencies [38].

To map the cytoplasmic viscoelastic response of living cells in detail, we performed intracellular optical tweezers measurements over a broad range of timescales (0.02–350 Hz) in fibroblast and macrophage cells. We modified the dynamic crosslinking model proposed by Lieleg *et al.* in Ref. [31] by adding a second dynamic crosslinking term, and found that the two-crosslinker model captures cytoplasmic mechanical behavior over the entire experimental frequency range for multiple cell types. The two unbinding rates observed may be due to multiple independent crosslinkers which dominate the timescales of the cell's viscoelastic response, or alternatively may be due to a single dominant crosslinker with multiple states which lead to two unbinding rates. The model provides insight into the physiological mechanisms of cellular viscoelasticity and offers a theoretical framework to analyze and understand cell mechanics.

## II. METHODS

### A. Cell culture and slide preparation

Macrophages (J774.1, ATTC) and wild-type immortalized dermal fibroblasts [39] were cultured in complete Dulbecco's Modified Eagle Medium (DMEM) media (Thermo Fisher Scientific) supplemented with 2 mM GlutaMAX (Thermo Fisher Scientific), 10% Fetal Bovine Serum (FBS) (Thermo Fisher Scientific), 100 U/mL penicillin, and 100 ug/mL streptomycin. Fibroblasts were passaged at ∼80% confluency via trypsinization and terminated by P20. Macrophages were passaged at ∼70% confluency via scraping and terminated by P20. Cells were seeded onto glass coverslips 24–36 h prior to experiments to yield an appropriate cell density for mechanical measurements, minimizing cell-cell contacts.

Prior to cell seeding, 500-nm fluorescent carboxylated polystyrene beads (Thermo Fisher Scientific) were PEGylated following Ref. [40] to minimize interaction with cytoskeletal proteins and motors, and then washed and resuspended in hypertonic complete media (∼$10^7$ beads per mL, 10% Polyethylene Glycol (PEG) 3500, 0.25 M sucrose). The cells were incubated in the hypertonic media for 1 h to allow bead uptake via phagocytosis, followed by a $< 3-$min incubation in hypotonic media (2:3 water:complete media) to burst the phagosome membranes around the beads. The cells were then left to recover in regular complete media for at least 1 h prior to measurements.

A flow chamber was constructed on a glass microscope slide using double-sided tape and vacuum grease (Dow Corning) to mount the cell coverslip. Vacuum grease was used to seal the ends of the slide and prevent imaging media (Leibovitz) from evaporating during measurements. Measurements were taken at 37 ˚C using a custom-built environmental chamber with a heater (World Precision Instruments) and did not exceed 2 h.

### B. Mechanical measurements

We performed optical trap-based active microrheology [41] using the multicomponent excitation method we developed previously [38]. The optical trap was built on an inverted microscope (Ti-E: Nikon, 1.49 numerical aperture oil-immersion 100× objective) with a near-IR laser beam (1064 nm, 10 W, IPG Photonics), which was expanded to overfill the back aperture of the objective. The position of an intracellular trapped bead [Fig. 1(a)] relative to the trap center was recorded on a quadrant photodiode (QPD) (Thorlabs) via back focal plane interferometry. A 22-frequency excitation sine wave was applied to the trap via an optoacoustic deflector (AA Optoelectronics, DTSXY-400-1064, direct digital synthesizer driver) controlled through a field-programmable gate array and custom LabVIEW programs (National Instruments). The frequencies of excitation were chosen to cover the frequency range from ∼0.02 to 1000 Hz without significant overlap of the fundamental or harmonic frequencies. The amplitude of the wave at each frequency ranges from 1 to 50 nm and was chosen to provide a coherent signal while maintaining a linear response (primary response is $> 20$ dB above harmonic responses). Measurements were recorded for ∼275 s at 20 kHz to obtain sufficient data to calculate the mechanical moduli at the lowest measured frequency.

### C. Measurement processing and model fitting

The optical trap stiffness (pN/nm) and photodiode sensitivity (nm/V) were calibrated per measurement by fitting a simplified viscoelastic model simultaneously to the transfer function (TF) between the bead and trap motion and the power spectrum (PS) of the bead motion using MATLAB's lsqcurvefit function, as described in Ref. [42] [Figs. 1(c)–1(e)]. Only the portion of the data which can be approximated using this model was used for calibration, corresponding to data $> 1$ Hz in the TF and ∼10–1000 Hz in the PS. Where possible, a step excitation was used to directly estimate the QPD sensitivity (Supplemental Material, Fig. S1 [43]) [44]. The mechanical moduli were then calculated from the calibrated TF following Ref. [36] for all measured frequencies $< 500$ Hz where the coherence between the bead and trap signal is $> 90\%$ (Supplemental Material [43]). Using the response only at applied frequencies minimizes the contribution of thermal noise or active cellular processes to the bead movement (and thereby the calculated mechanics), as the magnitude of the bead movement due to laser oscillation at these specific frequencies is large in comparison to random movement. The mean and 95% confidence intervals were obtained by generating 1000 bootstrap samples with replacement from the measurement pool (31 unique measurements for the fibroblasts, 49 for the macrophages).

The mechanical models were fit to the mean data using MATLAB's lsqcurvefit function. For models with many free parameters ($> 5$), groups of parameters were fit iteratively to ensure optimal model fits (Supplemental Material, Fig. S2 [43]). To estimate the confidence of the model fitting, 1000 fits were generated by subjecting the initial parameter starting point to uniformly distributed random perturbations between $+/-25\%$. The resulting fit distributions were used to find the means and 95% confidence intervals (CIs) for model parameters and Bayesian information criterion (BIC) values. For parameters with no substantial variation, 95% CIs are not reported.

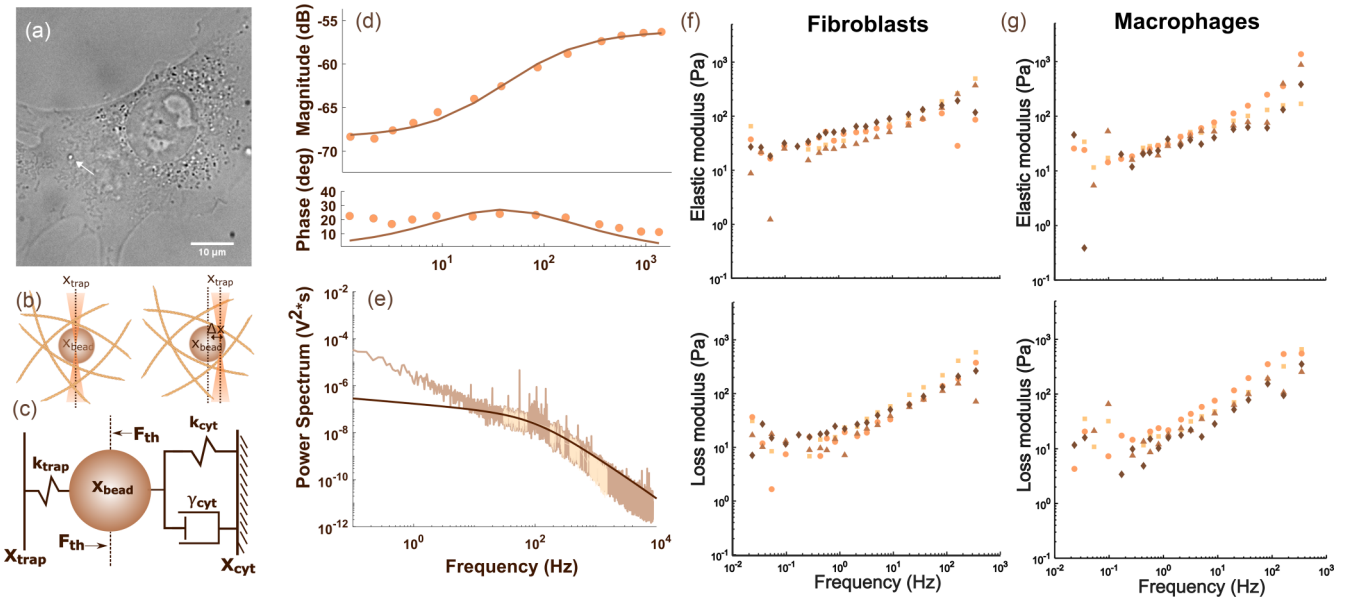


FIG. 1. Experimental setup and sample data. (a) Bright-field image of a fibroblast cell with a trapped bead (arrow). (b) Schematic of bead and laser motion during laser oscillation. As the laser is oscillated, the motion of the bead is impeded by its surrounding, causing it to deviate from the center of the trap (right). (c) Diagram depicting the forces acting on the bead due to the trap and viscoelastic environment. Cytoplasmic stiffness $k_{cyt}$ consists of two components, a constant elasticity ($k_{cyt,0}$) and a frequency-dependent elasticity ($k_{cyt,1}$). (d) Theoretical transfer function expression [Supplemental Material, Eq. (S3) [43]] is fit (brown line) to the transfer function between the bead and trap motion to obtain the unknown system parameters, including the trap stiffness ($k_{trap}$). (e) Theoretical power spectrum expression (Supplemental Material, Eq. (S4) [43]] is fit (dark brown line) to the power spectrum of the bead's motion to obtain the system's unknown parameters. The power spectrum represents the bead's thermal motion and is taken in the lateral direction perpendicular to the trap movement. Both the transfer function (magnitude and phase) and power spectrum are fit simultaneously to the data using MATLAB's lsqcurvefit function (Supplemental Material [43]). (f) Mechanical moduli from four individual fibroblast and (g) macrophage cells taken during four different experimental sessions.

## III. RESULTS

Previously, we showed that the cytoplasm of fibroblast cells exhibits a transition to fluidlike behavior at long timescales [38], consistent with the dynamic crosslinking model proposed by Lieleg *et al.* [31]. However, additional measurements were needed to map the low-frequency mechanics with adequate resolution to constrain mathematical models. Here, we measured the frequency-dependent mechanical response of fibroblasts and macrophages with high-resolution using intracellular optical trap-based microrheology [38,41], including additional excitation frequencies to better resolve mechanics at slow timescales (see Methods (Sec. II) and Fig. 1).

Reported measurements of the viscoelastic response of the cytoplasm in living cells vary considerably due to differences in cell types, culture conditions, and experimental techniques. While many measurements of cell mechanics in the literature are consistent with power-law behavior [19,21,45–49], other measurements show deviation from power-law behavior at low frequencies [37,38,50]. Here, we find that a power law [Eqs. (1) and (2)] using two exponents ($\alpha$, $\beta$) to describe two frequency-dependent regimes fails to accurately capture the mechanics of both macrophages and fibroblasts at slow timescales [< 1 Hz, Figs. 2(b) and 2(c)]. While the data do show broad trends consistent with previously reported cellular power-law mechanics [21,47–49], with a low-frequency exponent near 0.2 and a high-frequency exponent approaching 1 (Table I), the model clearly fails to capture the low-frequency response [Figs. 2(b) and 2(c)]. Given the distinct minima and maxima observed at the lower frequencies, it appears that the mechanical behavior in this frequency range is governed by phenomena which lead to distinct relaxation timescales, explaining the inability of the power-law model to describe this response.

We next fit the dynamic crosslinking model proposed by Lieleg *et al.* to our viscoelastic response measurements, given in Eqs. (3) and (4) [31]. This model accounts for a plateau elastic modulus ($G_0$) and a single crosslinker unbinding rate ($k_{off}$), as well as a power-law frequency regime with dynamics governed by an exponent $\beta$. The crosslinker unbinding rate gives a local maximum in the viscous response as energy is effectively dissipated via network rearrangement, and a corresponding local decrease in the elastic response [31]. However, the single-$k_{off}$ DCM [Fig. 2(a)] was also unable to capture the broad relaxation dynamics observed and offered only a slightly better characterization of the responses than the power-law model [Figs. 2(b) and 2(c)]. In response, we extended the DCM to include two dominant crosslinkers with different unbinding kinetics [Eqs. (5) and (6), Supplemental Material [43]). The double-$k_{off}$ DCM includes the same parameters as the single-$k_{off}$ DCM with the addition of a second crosslinker unbinding rate, $k_{off2}$, thus providing a model with two timescales of relaxation [Fig. 2(a)]. This model was able

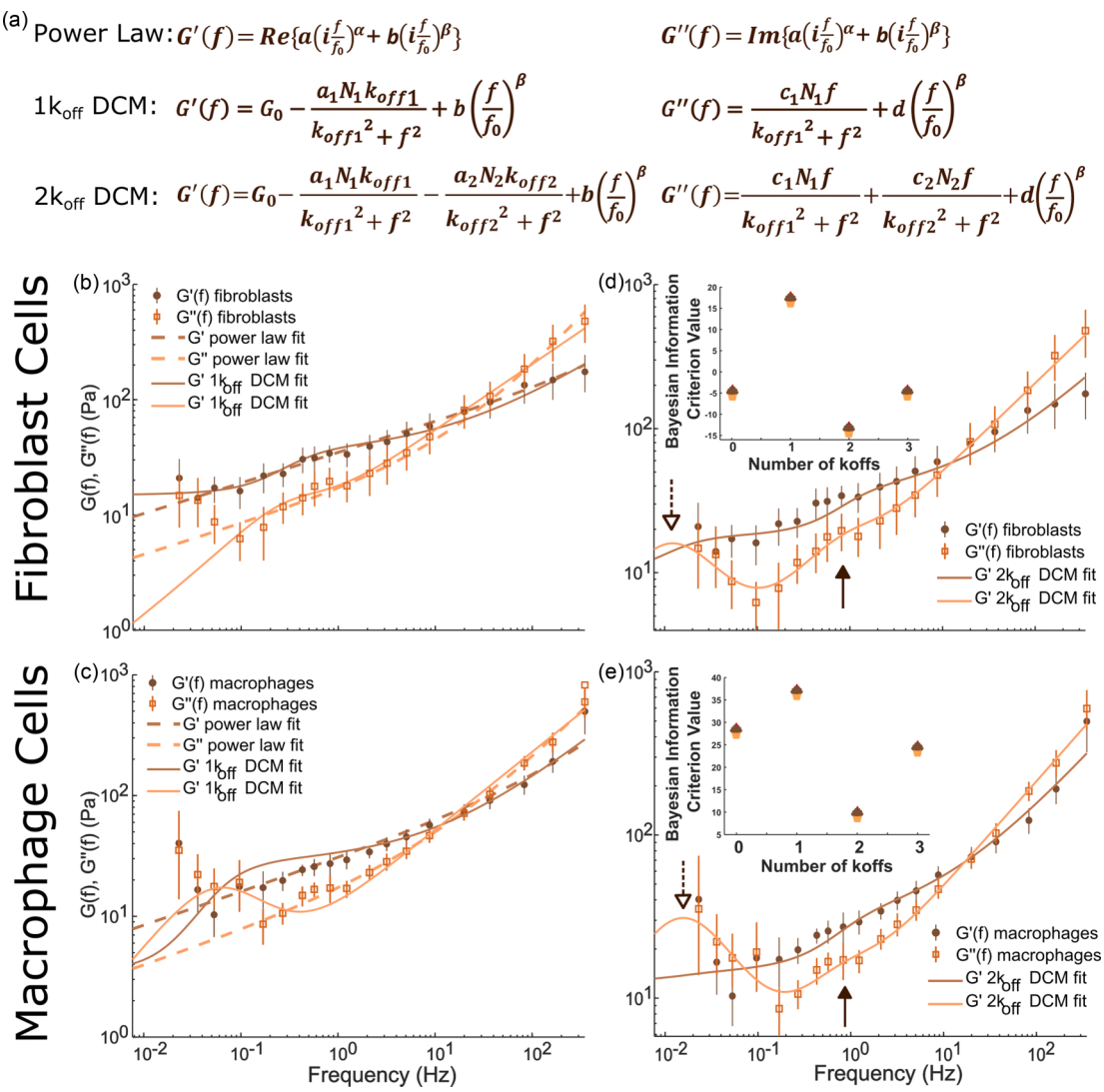


FIG. 2. Mechanics of fibroblasts and macrophages follow a double-unbinding rate dynamic crosslinking model. (a) Analytical expressions for the elastic ($G'$) and viscous ($G''$) modulus in the double power-law model, 1-$k_{off}$ dynamic crosslinking model, and 2-$k_{off}$ dynamic crosslinking model. a–d represent scaling constants; $N_1$ and $N_2$ are the number of crosslinkers in the system with unbinding rates of $k_{off1}$ and $k_{off2}$, respectively; $\alpha$, $\beta$ control the frequency dependence of the power-law terms; and $f_0$ determines the frequencies at which the power-law terms become predominant. (b) Viscoelastic response of fibroblasts (mean ± 95% CI from 1000 bootstrapped samples) and (c) macrophages cannot be described by the power-law model (dashed) or 1-$k_{off}$ DCM (solid), as both fail to simultaneously characterize the low- and intermediate frequency response. (d) Both the fibroblast and (e) macrophage data sets are well described by a 2-$k_{off}$ DCM, with similar fast (solid arrow) and slow (dashed arrow) crosslinker unbinding rates. Insets show normalized BIC value for models with 0–3 $k_{off}$ terms (0 = power−law model). ($n = 31$ fibroblasts, 49 macrophages).

to characterize the observed behavior over the entire frequency range, as it provides a framework capable of capturing the relaxation rates seen at both the low and intermediate frequencies [Figs. 2(d) and 2(e)]. Adding a third $k_{off}$ term to the dynamic crosslinking model did not further improve the model fit to the data [Figs. S3(e)–S3(h), Table S2, [43]].

$$G'(f) = \mathrm{Re}\left(a\left(i\frac{f}{f_0}\right)^\alpha + b\left(i\frac{f}{f_0}\right)^\beta\right), \quad (1)$$

$$G''(f) = \mathrm{Im}\left(a\left(i\frac{f}{f_0}\right)^\alpha + b\left(i\frac{f}{f_0}\right)^\beta\right), \quad (2)$$

$$G'(f) = G_0 - \frac{a_1 N_1 k_{\mathrm{off}1}}{k_{\mathrm{off}1}^2 + f^2} + b\left(\frac{f}{f_0}\right)^\beta, \quad (3)$$

$$G''(f) = \frac{c_1 N_1 f}{k_{\mathrm{off}1}^2 + f^2} + d\left(\frac{f}{f_0}\right)^\beta, \quad (4)$$

$$G'(f) = G_0 - \frac{a_1 N_1 k_{\mathrm{off}1}}{k_{\mathrm{off}1}^2 + f^2} - \frac{a_2 N_2 k_{\mathrm{off}2}}{k_{\mathrm{off}2}^2 + f^2} + b\left(\frac{f}{f_0}\right)^\beta, \quad (5)$$

$$G''(f) = \frac{c_1 N_1 f}{k_{\mathrm{off}1}^2 + f^2} + \frac{c_2 N_2 f}{k_{\mathrm{off}2}^2 + f^2} + d\left(\frac{f}{f_0}\right)^\beta. \quad (6)$$

We used Bayesian information criteria (BIC) to quantitively compare the candidate models and account for their varying complexity [51]. The 2-$k_{off}$ DCM has the lowest information criterion value of all models in both cell types when comparing the BIC values obtained using normalized resid-

TABLE I. Model parameter and BIC values for models fit to the cytoplasmic viscoelastic response. Frequency-dependence parameters represent variables which control how the mechanics vary in response to frequency, while scaling constants adjust the magnitude of the mechanical moduli. Numbers in brackets represent 95% confidence intervals (provided where relevant). $f_0 = 1$ for all models.

| | Power law (fibroblasts) | Power law (macrophages) | 1-$k_{off}$ DCM (fibroblasts) | 1-$k_{off}$ DCM (macrophages) | 2-$k_{off}$ DCM (fibroblasts) | 2-$k_{off}$ DCM (macrophages) |
|---|---|---|---|---|---|---|
| Frequency - dependence parameters | | | | | | |
| $\alpha$ | 0.264 | 0.275 | | | | |
| $\beta$ | 0.953 | 0.836 | 0.574 | 0.647 | 0.621<br>[0.616, 0.624] | 0.647 |
| $k_{off1}$ $(Hz)$ | | | 0.333<br>[0.331, 0.334] | 0.0597 | 0.011 6<br>[0.006 30, 0.019 6] | 0.0153<br>[0.013 5, 0.017 2] |
| $k_{off2}$ $(Hz)$ | | | | | 0.936<br>[0.743, 1.17] | 0.878<br>[0.756, 1.05] |
| *Scaling constants* | | | | | | |
| $G_0$ $(Pa)$ | 34.0 | 27.5 | 34.0 | 27.5 | 34.0 | 27.5 |
| $a$ $(Pa)$ | 38.0 | 33.0 | | | | |
| $b$ $(Pa)$ | 1.92 | 3.61 | 5.97 | 5.87 | 5.03<br>[4.97, 5.15] | 6.60<br>[6.56, 6.66] |
| $d$ $(Pa)$ | | | 14.5<br>[14.5, 14.6] | 11.7 | 11.9<br>[11.6, 12.2] | 10.9<br>[10.8, 11.0] |
| $a_1N_1$ $(Pa\,Hz)$ | | | 1.02<br>[1.02, 1.03] | 0.229 | 0.0138<br>$[0.306,\ 2.98] \times 10^{-2}$ | 0.003 25<br>$[2.72,\ 3.91] \times 10^{-3}$ |
| $a_2N_2$ $(Pa\,Hz)$ | | | | | 2.44<br>[2.04, 2.83] | 1.89<br>[1.65, 2.23] |
| $c_1N_1$ $(Pa\,Hz)$ | | | 3.89<br>[3.84, 3.96] | 1.83 | 0.351<br>[0.314, 0.412] | 0.920<br>[0.885, 0.960] |
| $c_2N_2$ $(Pa\,Hz)$ | | | | | 13.7<br>[9.93, 18.1] | 10.1<br>[8.25, 12.9] |
| *Information criteria* | | | | | | |
| $BIC$ $(norm)$ | −4.93 | 27.9 | 17.0 | 36.4 | −14.2<br>[−19.6, −6.51] | 9.42<br>[8.79, 10.4] |
| $BIC$ $(raw)$ | 341 | 401 | 335<br>[335, 336] | 406 | 334<br>[330, 337] | 411 |

uals, such that the data are weighted approximately equally across the frequency range [Figs. 2(d) and 2(e); Table I]. Interestingly, this advantage becomes less apparent when comparing BIC values obtained using raw residuals, which naturally weigh the higher-frequency data more heavily due to their larger magnitude. This indicates that while a power law or 1-$k_{off}$ DCM may be suitable to describe the cell's viscoelastic response in cases where high-frequency data are the primary focus, these models are incapable of accurately capturing the cell's slower frequency behavior.

Within the 2-$k_{off}$ DCM, both the fibroblasts and macrophages showed comparable behavior, with similar power-law exponents ($\sim 0.6$) and crosslinker unbinding rates ($k_{off2}$ ~0.9 Hz and $k_{off1} \sim 0.01$ Hz). The values for the parameters of all the models fit to the data are given in Table I. Note that the estimates for $k_{off1}$ are based on the position of the low-frequency peak in the loss modulus, which lies at the edge of the experimental range. Measuring the response at low frequencies poses significant challenges due to the long measurement duration required to obtain several periods of measurement while active processes are ongoing in the cell, leading to a high degree of variance in the moduli at the lower frequencies and therefore a high degree of uncertainty in the estimates of the slower unbinding rate ($k_{off1}$). In particular, PEG-coated beads were more susceptible to interactions with motor proteins in macrophage cells, and beads were often pulled out of the trap prior to the end of the measurement. In addition, crowded cytoplasmic environments often led to beads being jostled out of the trap center prematurely, limiting the measurement length which can be reliably obtained and reducing the availability of data at the slower frequencies. This limited our ability to capture the cells' slower dynamics, and more reliable $k_{off1}$ estimates would require additional experiments to better delineate the mechanics at slow timescales. The 2-$k_{off}$ DCM fits obtained when excluding the slowest frequency data are similar to those in Fig. 1, and are provided in the Supplemental Material [Figs. S3(c) and S3(d); Table S1 [43]].

While using an active intracellular microrheological approach allowed us to obtain detailed measurements of the cytoplasmic mechanics at a wide range of frequencies, optical tweezer-based microrheology has several limitations. Beads may interact nonspecifically with cellular components, or cause reorganization of the cytoplasm and cytoskeleton. Using endogenous probes like lipid droplets could alleviate these limitations, but introduces other difficulties, such as uncontrolled interactions between the mechanical probe and the cytoskeleton, difficulties in trap calibration due to the

uncertain size of the probe, and the inability to exert adequate forces due to their size and refractive index [52]. We therefore opted to introduce probe beads via phagocytosis, followed by an osmotic shock to lyse phagosomes and release passivated beads into the cytoplasm. Cells were then allowed to recover from the probe uptake procedure before undergoing mechanical measurements [see Methods (Sec. II)] [38]. However, any intracellular probe necessitates an *in situ* trap calibration, as the trap strength varies from cell to cell and probe to probe due to their varying optical properties [38,42,53]. Finally, the use of a high-powered laser to trap the probes causes a local increase in the intracellular temperature and could alter diffusion and protein binding kinetics, influencing the measured mechanics and estimates reported for $k_{\text{off}}$ [29,54–57]. The trap wavelength was therefore chosen to have low absorption in biological tissue [58] and measurements were kept under 5 min in duration to minimize the effects of local heating. Despite the above limitations, optical tweezer-based microrheology provides high-resolution maps of the frequency-dependent viscoelastic properties of the cytoplasm due to their high sensitivity ($< 0.1$ pN, $< 1$ nm) and ability to probe mechanics over a broad range of timescales, from microseconds to minutes.

## IV. DISCUSSION

The inability of the power-law model to describe the cell's low-frequency viscoelastic behavior indicates that the mechanics of the cytoplasm are governed by distinct phenomena over low and high frequencies, with cytoskeletal crosslinker unbinding dynamics governing low-frequency mechanics and cytoskeletal filament dynamics governing only the cell's high-frequency response [24,31]. The proposed 2-$k_{\text{off}}$ model [Fig. 2(a)] does not differ significantly from pure power-law models at high frequencies, as the crosslinkers remain statically bound to the network at these timescales [Fig. 3(a)] and the mechanical behavior is governed chiefly by filament fluctuations, which are accounted for by the power-law term [Fig. 3(d)]. However, at intermediate frequencies, the mechanics begin to deviate from power-law behavior, as can be seen by a peak in the viscous modulus and a decrease in the elastic modulus [Fig. 3(e)]. This occurs at $k_{\text{off}2}$, when the crosslinkers with a dissociation rate of $k_{\text{off}2}$ are unbinding and allowing some cytoskeletal rearrangement to occur [Fig. 3(b)]. The effect of $k_{\text{off}2}$ on the mechanical response becomes less distinct as $k_{\text{off}2}$ becomes faster, since the broad range of relaxation timescales present at high frequencies prevents the contribution of individual relaxation rates from being observable [Fig. 3(e)]. At very low frequencies, the second population of crosslinkers begins to unbind at a rate of $k_{\text{off}1}$ [Fig. 3(c)], leading to another maximum in the viscous modulus and dip in the elastic modulus at $k_{\text{off}1}$ [Fig. 3(f)].

Several possible mechanisms might lead to the observation of two distinct unbinding rates. Although a multitude of cytoskeletal crosslinkers has been identified to date [59–63], obtaining reliable estimates for their unbinding rates is experimentally challenging and estimates vary widely by technique [64–66]. However, several have been found to have unbinding rates on the order of magnitude of the rates reported here, and suggest that the unbinding rates of many crosslinkers may be too similar to one another to be distinct in the cell's viscoelastic response [Figs. 3(e) and 3(f)] [64,67–70]. In this case, $k_{\text{off}1}$ and $k_{\text{off}2}$ would represent the ensemble average unbinding rates of two dominant groups of cytoskeletal crosslinkers controlling the timescales of cytoplasmic mechanics [Fig. 4(a)]. However, it is also possible that only a select few of the large variety of crosslinkers in the cytoplasm have a significant effect on the cell's viscoelastic response in the frequency range being studied. While the mechanical role of certain cytoskeletal crosslinkers has been studied (often in simplified reconstituted systems), the exact contribution of each cytoskeletal-binding protein to the cell's mechanical response for the large part remains unknown [38,66,71–73], and it is therefore possible that many do not have a measurable effect on cytoplasmic mechanics. In this case, the two unbinding rates may be due only to the two crosslinkers with

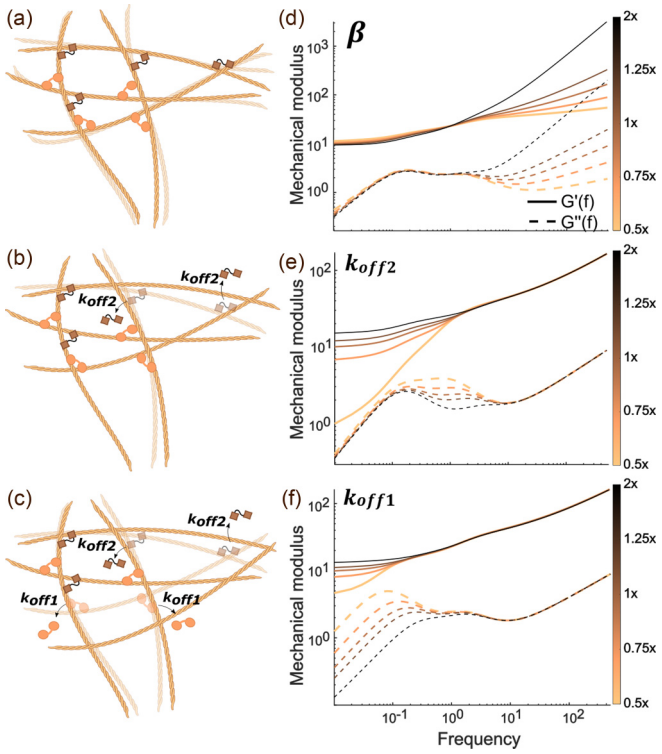


FIG. 3. Network behavior and corresponding mechanics over different timescales in the double-unbinding rate dynamic crosslinking model. (a) At frequencies $\gg k_{\text{off}2}$, the crosslinked network is static, and the mechanics are governed by entropic filament fluctuations. (b) At frequencies near $k_{\text{off}2}$, some cytoskeletal crosslinkers are unbinding, allowing for limited network rearrangement. (c) At frequencies $< k_{\text{off}1}$, all cytoskeletal crosslinkers are unbinding and allowing for network rearrangements, leading to an increase in fluidlike behavior. d) Increasing beta ($0.5x$–$2x$, light orange to brown) increases the frequency dependence of the elastic (solid lines) and viscous (dashed lines) modulus at high frequencies. (e) Increasing $k_{\text{off}2}$ (orange to brown) shifts the intermediate peak in the viscous and drop in the elastic modulus to higher frequencies. (f) Increasing $k_{\text{off}1}$ (orange to brown) shifts the leftmost peak in the viscous and drop in the elastic modulus to higher frequencies.

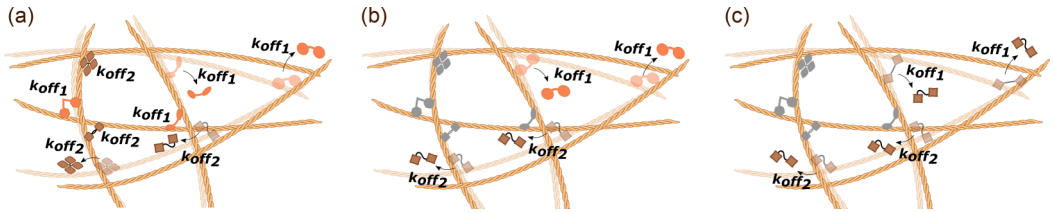


FIG. 4. Possible explanations for the two unbinding rates governing cytoplasmic mechanics. (a) Cytoskeletal crosslinkers fall into two categories: a slow-unbinding group (orange) and fast-unbinding group (brown). These two groups of cytoskeletal crosslinkers (orange, brown) govern the two relaxation rates of the cytoplasmic viscoelastic response. (b) Out of the cell's multitude of different cytoskeletal crosslinkers (orange, brown, gray), only two crosslinkers play a significant role in determining the cell's mechanical response (orange, brown). Each of the two dominant crosslinkers governs one of the relaxation rates of the cell's viscoelastic response. (c) Out of the cell's multitude of different cytoskeletal crosslinkers (brown, gray), only a single dominant cytoskeletal crosslinker plays a significant role in determining the cell's mechanical response (brown). This crosslinker exhibits two conformational states (straight linker, bent linker), leading to the two unbinding rates governing the relaxation rates of the cytoplasmic viscoelastic response.

the strongest influence on the cell's viscoelastic properties [Fig. 4(b)].

Finally, a third possibility is that these are in fact two unbinding rates of a single dominant cytoskeletal crosslinker [Fig. 4(c)]. Certain cytoskeletal crosslinkers can switch between conformational states and thereby change their binding kinetics [74]. This can be caused by regulatory factors which operate to switch the crosslinker between conformational states with fast and slow unbinding rates, or an intrinsic load dependence which causes it to unbind with increasing frequency in response to increasing tension (slip bond) or decreasing frequency in response to increasing tension (catch bond) [74–79].

The agreement between our data and the DCM model fit suggests that dynamic cytoskeletal crosslinkers are a major contributor to cytoplasmic mechanics at low frequencies. However, there are many components which contribute to the cytoplasmic viscoelastic response, including membranes, different cytoskeletal filaments, cytoskeletal motor proteins, cytosolic fluid, and the interactions between these components [17,26,39,80–87]. Simple models like the 2-$k_{\text{off}}$ DCM proposed here provide a framework for interpreting future research investigating the function of individual cytoskeletal elements and crosslinkers.

## V. CONCLUSION

Detailed measurements of the cell's low-frequency viscoelastic response using active microrheology reveal that the power-law model is incapable of capturing the cell's cytoplasmic mechanical behavior at slow timescales. In contrast to the broad range of relaxation timescales described by power laws, the cell exhibits two distinct relaxation rates, one at low (∼0.01 Hz) and one at intermediate (∼0.9 Hz) frequencies. The observation of these relaxation timescales in both macrophage and fibroblast cell types suggests that cytoskeletal crosslinker unbinding is a conserved mechanism controlling the frequency dependence of low-frequency cytoplasmic mechanical behavior, which can be described using a double-unbinding rate dynamic crosslinking model. The proposed model provides a theoretical framework to understand the physiological basis for the cell's viscoelastic response, elucidating the unique physiological factors regulating low-frequency and high-frequency mechanics. Further work is required to identify the main crosslinkers responsible for regulating the cell's viscoelastic relaxation rates as well as the components of the cytoskeleton with which they interact. This could provide crucial insight into the cell's mechanical regulatory system and further our understanding of diseases associated with abnormal mechanical properties.

## ACKNOWLEDGMENTS

The authors thank Loïc Chaubet and Emily Prowse for sharing their technical expertise and providing insightful feedback. O.T.C. was supported by Fonds de Recherche du Québec–Nature et Technologies (NSERC Undergraduate Summer Research Award supplement). A.G.H. acknowledges support from the Natural Sciences and Engineering Research Council of Canada (Grant No. RGPIN-2020-04608), and the Canadian Foundation for Innovation (Project 32749).

[1] G. B. Nash, E. O'Brien, E. C. Gordon-Smith, and J. A. Dormandy, Abnormalities in the mechanical properties of red blood cells caused by Plasmodium falciparum, Blood **74**, 855 (1989).

[2] J. Jaffar, S.-H. Yang, S. Y. Kim, H.-W. Kim, A. Faiz, W. Chrzanowski, and J. K. Burgess, Greater cellular stiffness in fibroblasts from patients with idiopathic pulmonary fibrosis, Am. J. Physiol.-Lung Cell. Mol. Physiol. **315**, L59 (2018).

[3] N. L. Sehgel, S. F. Vatner, and G. A. Meininger, Smooth muscle cell stiffness syndrome-revisiting the structural basis of arterial stiffness, Front. Physiol. **6**, 335 (2015).

[4] F. Lautenschläger, S. Paschke, S. Schinkinger, A. Bruel, M. Beil, and J. Guck, The regulatory role of cell mechanics for migration of differentiating myeloid cells, Proc. Natl. Acad. Sci. USA **106**, 15696 (2009).

[5] R. R. Chaturvedi, T. Herron, R. Simmons, D. Shore, P. Kumar, B. Sethia, F. Chua, E. Vassiliadis, and J. C. Kentish, Passive

stiffness of myocardium from congenital heart disease and implications for diastole, Circulation **121**, 979 (2010).

[6] K. A. Ward, W. I. Li, S. Zimmer, and T. Davis, Viscoelastic properties of transformed cells: Role in tumor cell progression and metastasis formation, Biorheology **28**, 301 (1991).

[7] J. H. Dangaria and P. J. Butler, Macrorheology and adaptive microrheology of endothelial cells subjected to fluid shear stress, Am. J. Physiol.-Cell Physiology **293**, C1568 (2007).

[8] R. Matzke, K. Jacobson, and M. Radmacher, Direct, high-resolution measurement of furrow stiffening during division of adherent cells, Nat. Cell Biol. **3**, 607 (2001).

[9] G. S. Worthen, B. Schwab, E. L. Elson, and G. P. Downey, Mechanics of stimulated neutrophils: Cell stiffening induces retention in capillaries, Science **245**, 183 (1989).

[10] H. Yu, C. Y. Tay, W. S. Leong, S. C. W. Tan, K. Liao, and L. P. Tan, Mechanical behavior of human mesenchymal stem cells during adipogenic and osteogenic differentiation, Biochem. Biophys. Res. Commun. **393**, 150 (2010).

[11] J. Hu, S. Jafari, Y. Han, A. J. Grodzinsky, S. Cai, and M. Guo, Size- and speed-dependent mechanical behavior in living mammalian cytoplasm, Proc. Natl. Acad. Sci. USA **114**, 9529 (2017).

[12] O. Thoumine and A. Ott, Time scale dependent viscoelastic and contractile regimes in fibroblasts probed by microplate manipulation, J. Cell Sci. **110**, 2109 (1997).

[13] T. L. Nguyen, E. R. Polanco, A. N. Patananan, T. A. Zangle, and M. A. Teitell, Cell viscoelasticity is linked to fluctuations in cell biomass distributions, Sci. Rep. **10**, 7403 (2020).

[14] E. Moeendarbary, L. Valon, M. Fritzsche, A. R. Harris, D. A. Moulding, A. J. Thrasher, E. Stride, L. Mahadevan, and G. T. Charras, The cytoplasm of living cells behaves as a poroelastic material, Nat. Mater. **12**, 253 (2013).

[15] A. Cartagena and A. Raman, Local viscoelastic properties of live cells investigated using dynamic and quasi-static atomic force microscopy methods, Biophys. J. **106**, 1033 (2014).

[16] N. Wang, K. Naruse, D. Stamenović, J. J. Fredberg, S. M. Mijailovich, I. M. Tolić-Nørrelykke, T. Polte, R. Mannix, and D. E. Ingber, Mechanical behavior in living cells consistent with the tensegrity model, Proc. Natl. Acad. Sci. USA **98**, 7765 (2001).

[17] B. D. Hoffman, G. Massiera, K. M. Van Citters, and J. C. Crocker, The consensus mechanics of cultured mammalian cells, Proc. Natl. Acad. Sci. USA **103**, 10259 (2006).

[18] Y. Bu, L. Li, and J. Wang, Power law creep and relaxation with the atomic force microscope: Determining viscoelastic property of living cells, Sci. China: Technol. Sci. **62**, 781 (2019).

[19] M. Balland, N. Desprat, D. Icard, S. Féréol, A. Asnacios, J. Browaeys, S. Hénon, and F. Gallet, Power laws in microrheology experiments on living cells: Comparative analysis and modeling, Phys. Rev. E Stat. Nonlin. Soft Matter Phys. **74**, 021911 (2006).

[20] E. H. Zhou, S. T. Quek, and C. T. Lim, Power-law rheology analysis of cells undergoing micropipette aspiration, Biomech. Model. Mechanobiol. **9**, 563 (2010).

[21] B. Fabry, G. N. Maksym, J. P. Butler, M. Glogauer, D. Navajas, and J. J. Fredberg, Scaling the Microrheology of Living Cells, Phys. Rev. Lett. **87**, 148102 (2001).

[22] S. Hurst, B. E. Vos, M. Brandt, and T. Betz, Intracellular softening and increased viscoelastic fluidity during division, Nat. Phys. **17**, 1270 (2021).

[23] C. P. Broedersz, M. Depken, N. Y. Yao, M. R. Pollak, D. A. Weitz, and F. C. MacKintosh, Cross-Link-Governed Dynamics of Biopolymer Networks, Phys. Rev. Lett. **105**, 238101 (2010).

[24] L. Deng, X. Trepat, J. P. Butler, E. Millet, K. G. Morgan, D. A. Weitz, and J. J. Fredberg, Fast and slow dynamics of the cytoskeleton, Nat. Mater. **5**, 636 (2006).

[25] K. K. Mandadapu, S. Govindjee, and M. R. K. Mofrad, On the cytoskeleton and soft glassy rheology, J. Biomech. **41**, 1467 (2008).

[26] O. Lieleg, K. M. Schmoller, M. M. A. E. Claessens, and A. R. Bausch, Cytoskeletal polymer networks: Viscoelastic properties are determined by the microscopic interaction potential of cross-links, Biophys. J. **96**, 4725 (2009).

[27] D. H. Wachsstock, W. H. Schwarz, and T. D. Pollard, Cross-linker dynamics determine the mechanical properties of actin gels, Biophys. J. **66**, 801 (1994).

[28] S. M. V. Ward, A. Weins, M. R. Pollak, and D. A. Weitz, Dynamic viscoelasticity of actin cross-linked with wild-type and disease-causing mutant $\alpha$-Actinin-4, Biophys. J. **95**, 4915 (2008).

[29] J. Xu, D. Wirtz, and T. D. Pollard, Dynamic cross-linking by $\alpha$-Actinin determines the mechanical properties of actin filament networks, J. Biol. Chem. **273**, 9570 (1998).

[30] N. Y. Yao, C. P. Broedersz, M. Depken, D. J. Becker, M. R. Pollak, F. C. MacKintosh, and D. A. Weitz, Stress-Enhanced Gelation: A Dynamic Nonlinearity of Elasticity, Phys. Rev. Lett. **110**, 018103 (2013).

[31] O. Lieleg, M. M. A. E. Claessens, Y. Luan, and A. R. Bausch, Transient Binding and Dissipation in Cross-Linked Actin Networks, Phys. Rev. Lett. **101**, 108101 (2008).

[32] M. Atakhorrami, G. H. Koenderink, J. F. Palierne, F. C. MacKintosh, and C. F. Schmidt, Scale-Dependent Nonaffine Elasticity of Semiflexible Polymer Networks, Phys. Rev. Lett. **112**, 088101 (2014).

[33] F. Gittes, B. Schnurr, P. D. Olmsted, F. C. MacKintosh, and C. F. Schmidt, Microscopic Viscoelasticity: Shear Moduli of Soft Materials Determined from Thermal Fluctuations, Phys. Rev. Lett. **79**, 3286 (1997).

[34] T. Golde, M. Glaser, C. Tutmarc, I. Elbalasy, C. Huster, G. Busteros, D. M. Smith, H. Herrmann, J. A. Käs, and J. Schnauß, The role of stickiness in the rheology of semiflexible polymers, Soft Matter **15**, 4865 (2019).

[35] T. G. Mason, T. Gisler, K. Kroy, E. Frey, and D. A. Weitz, Rheology of F-actin solutions determined from thermally driven tracer motion, J. Rheol. **44**, 917 (2000).

[36] D. Mizuno, D. A. Head, F. C. MacKintosh, and C. F. Schmidt, Active and passive microrheology in equilibrium and nonequilibrium systems, Macromolecules **41**, 7194 (2008).

[37] F. Wottawah, S. Schinkinger, B. Lincoln, R. Ananthakrishnan, M. Romeyke, J. Guck, and J. Käs, Optical Rheology of Biological Cells, Phys. Rev. Lett. **94**, 098103 (2005).

[38] L. Chaubet, A. R. Chaudhary, H. K. Heris, A. J. Ehrlicher, and A. G. Hendricks, Dynamic actin cross-linking governs the cytoplasm's transition to fluid-like behavior, Mol. Biol. Cell **31**, 1744 (2020).

[39] A. J. Ehrlicher, R. Krishnan, M. Guo, C. M. Bidan, D. A. Weitz, and M. R. Pollak, Alpha-actinin binding kinetics modulate cellular dynamics and force generation, Proc. Natl. Acad. Sci. **112**, 6619 (2015).

[40] M. T. Valentine, Z. E. Perlman, M. L. Gardel, J. H. Shin, P. Matsudaira, T. J. Mitchison, and D. A. Weitz, Colloid surface chemistry critically affects multiple particle tracking measurements of biomaterials, Biophys. J. **86**, 4004 (2004).

[41] D. Mizuno, R. Bacabac, C. Tardin, D. Head, and C. F. Schmidt, High-Resolution Probing of Cellular Force Transmission, Phys. Rev. Lett. **102**, 168102 (2009).

[42] A. G. Hendricks, E. L. F. Holzbaur, and Y. E. Goldman, Force measurements on cargoes in living cells reveal collective dynamics of microtubule motors, Proc. Natl. Acad. Sci. USA **109**, 18447 (2012).

[43] See Supplemental Material at http://link.aps.org/supplemental/10.1103/PhysRevResearch.4.043167 for supplemental methods and figures.

[44] J. R. Staunton, B. Blehm, A. Devine, and K. Tanner, In situ calibration of position detection in an optical trap for active microrheology in viscous materials, Opt. Express **25**, 1746 (2017).

[45] D. Stamenović, N. Rosenblatt, M. Montoya-Zavala, B. D. Matthews, S. Hu, B. Suki, N. Wang, and D. E. Ingber, Rheological behavior of living cells is timescale-dependent, Biophys. J. **93**, L39 (2007).

[46] J. Alcaraz, L. Buscemi, M. Grabulosa, X. Trepat, B. Fabry, R. Farré, and D. Navajas, Microrheology of human lung epithelial cells measured by atomic force microscopy, Biophys. J. **84**, 2071 (2003).

[47] B. Fabry, G. N. Maksym, J. P. Butler, M. Glogauer, D. Navajas, N. A. Taback, E. J. Millet, and J. J. Fredberg, Time scale and other invariants of integrative mechanical behavior in living cells, Phys. Rev. E Stat. Nonlin. Soft Matter Phys. **68**, 041914 (2003).

[48] G. Fläschner, C. I. Roman, N. Strohmeyer, D. Martinez-Martin, and D. J. Müller, Rheology of rounded mammalian cells over continuous high-frequencies, Nat. Commun. **12**, 2922 (2021).

[49] A. Rigato, A. Miyagi, S. Scheuring, and F. Rico, High-frequency microrheology reveals cytoskeleton dynamics in living cells, Nat. Phys. **13**, 771 (2017).

[50] J. R. Staunton, W. Y. So, C. D. Paul, and K. Tanner, High-frequency microrheology in 3D reveals mismatch between cytoskeletal and extracellular matrix mechanics, Proc. Natl. Acad. Sci. **116**, 14448 (2019).

[51] G. Schwarz, Estimating the dimension of a model, Ann. Stat. **6**, 461 (1978).

[52] C. Arbore, L. Perego, M. Sergides, and M. Capitanio, Probing force in living cells with optical tweezers: From single-molecule mechanics to cell mechanotransduction, Biophys. Rev. **11**, 765 (2019).

[53] A. G. Hendricks and Y. E. Goldman, Measuring molecular forces using calibrated optical tweezers in living cells, Methods Mol. Biol. **1486**, 537 (2017).

[54] C. Aermes, A. Hayn, T. Fischer, and C. T. Mierke, Cell mechanical properties of human breast carcinoma cells depend on temperature, Sci. Rep. **11**, 10771 (2021).

[55] C. J. Chan, G. Whyte, L. Boyde, G. Salbreux, and J. Guck, Impact of heating on passive and active biomechanics of suspended cells, Interface Focus **4**, 20130069 (2014).

[56] S. Ebert, K. Travis, B. Lincoln, and J. Guck, Fluorescence ratio thermometry in a microfluidic dual-beam laser trap, Opt. Express. **15**, 15493 (2007).

[57] T. R. Kießling, R. Stange, J. A. Käs, and A. W. Fritsch, Thermorheology of living cells—impact of temperature variations on cell mechanics, New J. Phys. **15**, 045026 (2013).

[58] J. Bixler, B. Hokr, M. Denton, G. Noojin, A. Shingledecker, H. Beier, R. Thomas, B. Rockwell, and V. Yakovlev, Assessment of tissue heating under tunable near-infrared radiation, J. Biomed. Opt. **19**, 70501 (2014).

[59] C. G. D. Remedios, D. Chhabra, M. Kekic, I. V. Dedova, M. Tsubakihara, D. A. Berry, and N. J. Nosworthy, Actin binding proteins: Regulation of cytoskeletal microfilaments, Physiol. Rev. **83**, 433 (2003).

[60] R. Mohan and A. John, Microtubule-associated proteins as direct crosslinkers of actin filaments and microtubules, IUBMB Life **67**, 395 (2015).

[61] Y. Yang, J. Dowling, Q. C. Yu, P. Kouklis, D. W. Cleveland, and E. Fuchs, An essential cytoskeletal linker protein connecting actin microfilaments to intermediate filaments, Cell **86**, 655 (1996).

[62] A. Bretscher, Fimbrin is a cytoskeletal protein that crosslinks F-actin in vitro, Proc. Natl. Acad. Sci. USA **78**, 6849 (1981).

[63] T. E. Kreis and R. E. Vale, *Guidebook to Cytoskeletal and Motor Proteins*, 2nd ed. (Oxford University Press, Oxford, 1999).

[64] J. M. Ferrer, H. Lee, J. Chen, B. Pelz, F. Nakamura, R. D. Kamm, and M. J. Lang, Measuring molecular rupture forces between single actin filaments and actin-binding proteins, Proc. Natl. Acad. Sci. **105**, 9221 (2008).

[65] W. H. Goldmann and G. Isenberg, Analysis of filamin and alpha-actinin binding to actin by the stopped flow method, FEBS Lett. **336**, 408 (1993).

[66] Y. Mulla, H. Wierenga, C. Alkemade, P. R. ten Wolde, and G. H. Koenderink, Frustrated binding of biopolymer crosslinkers, Soft Matter **15**, 3036 (2019).

[67] Z. Lansky, M. Braun, A. Lüdecke, M. Schlierf, P. R. ten Wolde, M. E. Janson, and S. Diez, Diffusible crosslinkers generate directed forces in microtubule networks, Cell **160**, 1159 (2015).

[68] Y. S. Aratyn, T. E. Schaus, E. W. Taylor, and G. G. Borisy, Intrinsic dynamic behavior of fascin in filopodia, Mol. Biol. Cell **18**, 3928 (2007).

[69] C. T. Skau, D. S. Courson, A. J. Bestul, J. D. Winkelman, R. S. Rock, V. Sirotkin, and D. R. Kovar, Actin filament bundling by fimbrin is important for endocytosis, cytokinesis, and polarization in fission yeast, J. Biol. Chem. **286**, 26964 (2011).

[70] T. P. Lele, J. Pendse, S. Kumar, M. Salanga, J. Karavitis, and D. E. Ingber, Mechanical forces alter zyxin unbinding kinetics within focal adhesions of living cells, J. Cell. Physiol. **207**, 187 (2006).

[71] Y. Tseng, T. P. Kole, J. S. Lee, E. Fedorov, S. C. Almo, B. W. Schafer, and D. Wirtz, How actin crosslinking and bundling proteins cooperate to generate an enhanced cell mechanical response, Biochem. Biophys. Res. Commun. **334**, 183 (2005).

[72] E. M. Reichl, Y. Ren, M. K. Morphew, M. Delannoy, J. C. Effler, K. D. Girard, S. Divi, P. A. Iglesias, S. C. Kuo, and D. N. Robinson, Interactions between myosin and actin crosslinkers

control cytokinesis contractility dynamics and mechanics, Curr. Biol. **18**, 471 (2008).

[73] M. L. Gardel, K. E. Kasza, C. P. Brangwynne, J. Liu, and D. A. Weitz, Chapter 19: Mechanical response of cytoskeletal networks, Methods Cell Biol. **89**, 487 (2008).

[74] E. Fuchs and I. Karakesisoglou, Bridging cytoskeletal intersections, Genes Dev. **15**, 1 (2001).

[75] L. Rognoni, J. Stigler, B. Pelz, J. Ylänne, and M. Rief, Dynamic force sensing of filamin revealed in single-molecule experiments, Proc. Natl. Acad. Sci. USA **109**, 19679 (2012).

[76] E. S. Schiffhauer, T. Luo, K. Mohan, V. Srivastava, X. Qian, E. R. Griffis, P. A. Iglesias, and D. N. Robinson, Mechanoaccumulative elements of the mammalian actin cytoskeleton, Curr. Biol. **26**, 1473 (2016).

[77] S. Le, X. Hu, M. Yao, H. Chen, M. Yu, X. Xu, N. Nakazawa, F. M. Margadant, M. P. Sheetz, and J. Yan, Mechanotransmission and mechanosensing of human alpha-Actinin 1, Cell Rep. **21**, 2714 (2017).

[78] K. Hosseini, L. Sbosny, I. Poser, and E. Fischer-Friedrich, Binding dynamics of $\alpha$-Actinin-4 in dependence of actin cortex tension, Biophys. J. **119**, 1091 (2020).

[79] D. L. Huang, N. A. Bax, C. D. Buckley, W. I. Weis, and A. R. Dunn, Vinculin forms a directionally asymmetric catch bond with F-actin, Science **357**, 703 (2017).

[80] M. G. Mendez, D. Restle, and P. A. Janmey, Vimentin enhances cell elastic behavior and protects against compressive stress, Biophys. J. **107**, 314 (2014).

[81] H. Ahmadzadeh, D. H. Smith, and V. B. Shenoy, Viscoelasticity of tau proteins leads to strain rate-dependent breaking of microtubules during axonal stretch injury: Predictions from a mathematical model, Biophys. J. **106**, 1123 (2014).

[82] M. Balland, A. Richert, and F. Gallet, The dissipative contribution of myosin II in the cytoskeleton dynamics of myoblasts, Eur. Biophys. J. **34**, 255 (2005).

[83] J. Hu, Y. Li, Y. Hao, T. Zheng, S. K. Gupta, G. A. Parada, H. Wu, S. Lin, S. Wang, X. Zhao, R. D. Goldman, S. Cai, and M. Guo, High stretchability, strength, and toughness of living cells enabled by hyperelastic vimentin intermediate filaments, Proc. Natl. Acad. Sci. **116**, 17175 (2019).

[84] Y.-C. Lin, G. H. Koenderink, F. C. MacKintosh, and D. A. Weitz, Control of non-linear elasticity in F-actin networks with microtubules, Soft Matter **7**, 902 (2011).

[85] S. N. Ricketts, M. L. Francis, L. Farhadi, M. J. Rust, M. Das, J. L. Ross, and R. M. Robertson-Anderson, Varying crosslinking motifs drive the mesoscale mechanics of actin-microtubule composites, Sci. Rep. **9**, 12831 (2019).

[86] M. H. Jensen, E. J. Morris, and D. A. Weitz, Mechanics and dynamics of reconstituted cytoskeletal systems, Biochim. Biophys. Acta **1853**, 3038 (2015).

[87] M. H. Jensen, E. J. Morris, R. D. Goldman, and D. A. Weitz, Emergent properties of composite semiflexible biopolymer networks, Bioarchitecture **4**, 138 (2014).